Utilization of Catechol End-Functionalized PMMA as a Macromolecular Coupling Agent for Ceramic/Fluoropolymer Piezoelectric Composites

Vincent Bouad, Alexandre Fadel, Saj Mohan, Arthur Hamieh, Jean-François Tahon, Joël Lyskawa, Patrice Woisel, Antonio Da Costa, Anthony Ferri, Rachel Desfeux, et al.

Utilization of Catechol End-Functionalized PMMA as Macromolecular Coupling Agent for Ceramic/Fluoropolymer Piezoelectric Composites

Vincent Bouad,[1,2] Alexandre Fadel,[3] Saj Mohan,[4] Arthur Hamieh,[1,5] Jean-François Tahon,[1] Joël Lyskawa,[1] Patrice Woisel,[1] Antonio Da Costa,[4] Anthony Ferri,[4] Rachel Desfeux,[4] Freddy Ponchel,[5] Denis Remiens,[5] Vincent Ladmiral[2] and Sophie Barrau[1]**

[1] Université de Lille, CNRS, INRAE, Centrale Lille, UMR 8207 - UMET - Unité Matériaux et Transformations, F-59000 Lille, France

[2] ICGM, Université de Montpellier, CNRS, ENSCM, Montpellier, France

[3] Université de Lille, CNRS, INRA, ENSCL, Université d'Artois, FR 2638 - IMEC -Institut Michel-Eugène Chevreul, F-59000 Lille, France

[4] Université d'Artois, CNRS, Centrale Lille, Université de Lille, UMR 8181 – UCCS – Unité de Catalyse et Chimie du Solide, F-62300 Lens, France

[5] IEMN-DOAE-CNRS UMR 8520, Université polytechnique Hauts-de-France (UPHF), F-59313 Valenciennes, France

KEYWORDS: Catechol end-functionalized polymers, PMMA, fluoropolymers, ceramic functionalization, composite, piezoelectric

ABSTRACT. An approach based on the use of a macromolecular coupling agent and aiming to improve the interfacial adhesion between piezoelectric ceramics and piezoelectric polymer matrix in piezoelectric composites is presented. PMMA bearing a catechol moiety was used as macromolecular coupling agent, as PMMA is known to be miscible to piezoelectric fluoropolymers and catechol groups can strongly bind to a large variety of surfaces. Thus entanglement between the PMMA chains and the amorphous segments of the fluoropolymer would ensure the desired interfacial adhesion. Well-defined PMMA was synthesized via RAFT polymerization using 2-cyano-2-propyl dodecyl trithiocarbonate as chain transfer agent. The PMMA ω-chain end was then functionalized with a catechol group via a one-pot aminolysis/thia-Michael addition procedure using a dopamine acrylamide (DA) derivative as Michael acceptor. The presence of the catechol moiety at the chain end of the PMMA was controlled by ^{1}H NMR and cyclic voltammetry measurements. The resulting PMMA-DA was then grafted onto the surface of a lead-free piezoelectric ceramic film (i.e. a thin film of H_2O_2-activated $(Bi_{0.5}Na_{0.5})TiO_3$ (BNT) with a large contact area). The increase of the water contact angle confirmed the efficiency of the grafting. A commercial piezoelectric copolymer P(VDF-*co*-TrFE) was then spin-coated onto the modified BNT surface to form a bilayer composite. The composite cross-section prepared by cryofracture was examined by scanning electron microscopy and revealed that the ceramic/polymer interface of the BNT-PMMA/P(VDF-*co*-TrFE) bilayer composite exhibits a much better cohesion than its counterpart composite prepared from non-modified BNT. Moreover, the grazing incidence wide-angle X-ray scattering confirmed that the copolymer crystal structure was not impacted by the presence of the PMMA-DA coupling agent. A strong piezoelectric response was locally detected by Piezoresponse Force Microscopy. This study highlights the potential of PMMA-DA to be used as macromolecular coupling agent to improve the ceramic/polymer interface in piezoelectric composite materials.

INTRODUCTION

Piezoelectric materials are remarkable materials possessing the ability of converting a mechanical energy into an electric energy (generation of electric charges when submitted to a mechanical stress) and vice versa (mechanical strain under electric field).[1] If the principle of piezoelectricity has been discovered many years ago and these materials widely used as sensors,[2,3] the interest for piezoelectric materials was recently renewed as they could offer remarkable solutions in energy harvesting devices.[4,5]

Lead Zirconate Titanate (PZT) is the most well-known piezoelectric ceramic[6] as it possesses a very high piezoelectric coefficient (d_{33} from 225 to 585 pC/N[7]). However, the presence of lead has significantly restricted its uses in favor to other piezoelectric ceramics such as Sodium Potassium Niobate (KNN), Barium Titanate (BT) or Bismuth Sodium Titanate (BNT) in spite of their lower piezoelectric coefficient (80 pC/N[8], 190 pC/N[9] and 94 pC/N[10] respectively).[11,12] While KNN and BT derivatives present interesting properties for sensor applications, in the case of low temperature actuator applications ($T < 100°C$), BNT appears to be a promising candidate as alternative to PZT.[13,14] However despite high piezoelectric responses, piezoelectric ceramics have inherent properties such as brittleness and poor shapability which limit their applications. To remediate to their mechanical limitations, Yamada et al. prepared one of the first piezocomposites based on the dispersion of piezoelectric nanoparticules of PZT in a polymer matrix of poly(urethane).[15] This composite combines the high piezoelectric response of ceramics with the high mechanical properties of polymers (high flexibility and low brittleness, young modulus of around 2 orders of magnitude lower than that of ceramics).

Polymers can also display such piezoelectric properties.[16,17] The most used piezoelectric polymer is poly(vinylidene fluoride) P(VDF).[18] This semi-crystalline polymer possesses different crystal phases, which differ on the spatial arrangement of the local dipolar moments generated by the highly polar C-F bonds.[19–21] In the β crystal phase, all the local dipoles are

oriented in the same direction, giving to the PVDF its highest electroactive properties. To obtain such a phase, PVDF requires specific treatments like stretching,[22,23] quenching from the melt[24] or solvent casting using N,N-dimethylformamide (DMF).[25,26] To circumvent this processing requirement, VDF is often copolymerized with other fluoromonomers such as Trifluoroethylene (TrFE) to generate P(VDF-*co*-TrFE) copolymers which crystallize directly in their electroactive crystal phase.[27,28] Piezoelectric copolymers possess valuable mechanical properties compared to ceramics but their ferroelectric and piezoelectric properties are inferior. Therefore, the preparation of ceramic/piezoelectric polymer composites combining the properties of both materials presents a growing interest.[29–31] However, the interface between the piezoelectric ceramics and the fluoropolymer matrix is not strong enough, probably due to the different nature of materials and is prone to the formation of cavities that can decrease the piezoelectric properties of the composites.[32,33] The addition of coupling agents such as dopamine, polydopamine or their derivatives such as nitrodopamine has been successfully used to reduce the interface issues, as dopamine exhibits a catechol moiety, a well-known adhesive groups that can easily and strongly bond to ceramics.[34–37] However, since the interactions between a single molecular coupling agent and the polymer matrix could be limited, the synthesis of a macromolecular coupling agent miscible with the polymer matrix and with a catechol group at its chain-end presents a growing interest.[32] Indeed, fluoropolymers are well-known to be miscible with poly(methyl methacrylate) (PMMA),[38–40] an inexpensive amorphous commodity polymer which can be produced with a wide range of techniques.

In this context, the present work is dedicated to the improvement of the ceramic/polymer interface of the BNT/P(VDF-*co*-TrFE) composite using an end-functionalized PMMA integrating a catechol terminal group. In order to properly probe these interfaces, bilayer composites exhibiting a large contact surface were investigated. Special attention was paid to

the efficiency of the PMMA-DA coupling agent at the interface and to the resulting local piezoelectric properties.

EXPERIMENTAL SECTION

Materials. Acryloyl chloride, dopamine hydrochloride, sodium carbonate ($NaCO_3$), sodium borate ($Na_2B_4O_7$, 10 H_2O), magnesium sulfate ($MgSO_4$), methyl methacrylate (MMA), hydrochloric acid (HCl), 2-cyano-2-propyl dodecyl trithiocarbonate (CPDT), n-butylamine (99% of purity), dimethylphenylphosphine (DMPP), triethylamine (> 99% of purity), toluene, ethyl acetate, ethanol, methanol, dimethylformamide (DMF) acetonitrile (CAN) Formamide, diiodomethane and Tetrabutylammonium hexafluorophosphate (Bu_4NPF_6)) were purchased from Sigma-Aldrich and used without any further purification. Azobisisobutyronitrile (AIBN) was recrystallized from methanol. Deuterated dimethylsulfoxyde (DMSO) and acetone were used as received from Eurisotop for ^{1}H NMR analysis. P(VDF-*co*-TrFE) (TrFE content = 20%mol, Mn = 200-320kDa, Đ = 2.6-2.9) was kindly supplied by Arkema.

Methods.

Nuclear Magnetic Resonance. Nuclear magnetic resonance (NMR) spectra were recorded on a Bruker AC 400 instrument. Deuterated acetone was used as the solvent in each sample. Coupling constants and chemical shifts are given in hertz (Hz). A one pulse 30° (4.76 μs) pulse sequence was used with 4 s acquisition time, 8 kHz spectral window centered at 3 kHz.

Size-Exclusion Chromatography. Size-exclusion chromatograms were recorded using a triple-detection 1260 Infinity II Multi-detector from Agilent Technologies with its corresponding Agilent software, dedicated to multidetector GPC calculation. The system used two PL1113-6300 ResiPore 300 × 7.5 mm columns with THF as the eluent with a flow rate of 1 mL.min^{-1} and toluene as the flow rate marker. The detector used was a 390-LC PL0390-0601

refractive index detector. The entire SEC-HPLC system was thermostated at 35°C. PMMA narrow standards were used for calibration (ranging from 500 to 1500000 g/mol). Typical sample concentration was 10 mg/mL.

Cyclo voltammetry. All electrochemical experiments (cyclic voltammetry) were performed using an Autolab PGSTAT 30 workstation. The electrolyte solution (0.05 M) was prepared from recrystallized tetrabutylammonium hexafluorophosphate (Bu_4NPF_6) and acetonitrile. A three-electrode configuration was used with a platinum disk (2 mm diameter) as working electrode, with an Ag/AgCl reference electrode and a platinum wire as the counter electrode. All measurements were recorded at 25°C under a nitrogen atmosphere. The solution was purged with nitrogen prior to electrochemical analyses.

Contact angle measurement. Water contact angles (WCA) and surface free energies (SFE) of the different surfaces were assessed with the sessile drop method on a DSA100 goniometer (Kruss: Villebon-sur-Yvette, France). WCA were measured on 2 mL droplets and SFE were calculated following the Owens, Wendt, Raeble and Kable (OWRK) method.[41] Formamide and diiodomethane were used as probe fluids. The results presented here are representative of at least three separate measurements on three different droplets randomly deposited on the surfaces.

SEM-EDX. For scanning electron microscopy (SEM) observations, cryofractured cross sections were prepared by plunging sample in liquid nitrogen and then by cutting with a diamond scraper. SEM images in secondary electron mode were recorded on carbon coated (around 20 nm) samples using a JEOL JSM-7800F LV. Energy Dispersive X-ray Spectroscopy (EDX) maps were also performed to identify the different ceramic and polymer layers using a X-Max SDD (Oxford Instruments) detector. Analytical conditions were 5 kV or 15kV accelerating voltage and 10 mm working distance.

GIWAXS. The Grazing Incidence Wide Angle X-ray scattering (GIWAXS) experiments were carried out using a Xeuss 2.0 (XENOCS) with a GeniX3D microsource (λ = 1.54 Å). The sample were put on the specific GIWAXS sample holder and the sample-to-detector distance was 160 mm. The acquisition time was 480s.

AFM. The surface and electrical properties of the P(VDF-*co*-TrFE) layer were locally characterized under ambient conditions by using Atomic Force Microscopy (AFM) and Piezoresponse Force Microscopy (PFM), respectively. The AFM topography was recorded in Tapping mode (TM-AFM) with a MultiMode instrument (Bruker Nano Inc., Santa Barbara, CA, USA), while both the electromechanical activity and the switching properties were probed with an MFP-3D instrument (Asylum Research/Oxford Instruments, USA). For PFM experiments (both in imaging and spectroscopic modes), Dual AC resonance tracking (DART)[42] method was employed for enhancing the piezoresponse signal, and a driving voltage (V_{AC}) of 1 V was applied between the conductive probe tip (PPP-EFM Pt/Ir-coated probes from NanoSensors, $k \approx 1.9$ N/m) and the ground substrate.

Syntheses and preparation of the bilayer composite.

Synthesis of N-(3,4-dihydroxyphenethyl)acrylamide (dopamine acrylamide) (DA). The synthesis of the DA (Scheme 1 (1)) was conducted using a protocol adapted from that reported by Detrembleur et al.[43] 4.0 g (10.5 mmol) of $Na_2B_4O_7 \cdot 10\ H_2O$ and 3.0 g (28.3mmol) of Na_2CO_3 in 100 mL of distilled water were degassed by nitrogen bubbling for 1h. 1.0 g (5.27 mmol) of dopamine hydrochloride was added to this solution and the reaction was allowed to proceed under stirring for 30 min. The reaction mixture was then cooled to 0°C before the dropwise addition of 2.7 mL (21.1 mmol) of acryloyl chloride. An additional 3.0 g of Na_2CO_3 was then added in order to keep the pH of the solution above 9 during the reaction. The reaction was stirred overnight at 30°C. The mixture was extracted 3 times with ethyl acetate, washed twice

with 0.1 M HCl and dried over $MgSO_4$, and purified by silica gel column chromatography using a dichloromethane:methanol (9:1) mixture as eluent.

^{1}H NMR (400Hz, Acetone d-6, Figure S1); δ(ppm)): 8.7 (s, 2H, -O**H$_j$**) 8.10 (t, J=5.6Hz, 1H, –N**H$_d$**–C=O), 6.62 (d, J_{ortho} = 7.9Hz, 1H, **H$_h$**), 6.57 (d, J_{meta} = 2.1Hz, 1H, **H$_i$**), 6.43 (dd, J_{ortho} = 7.9Hz; J_{meta} = 2.1Hz, 1H, **H$_g$**), 6.19 (dd, J_{cis} = 10.1Hz; J_{trans} = 17.1Hz, 1H, **H$_c$**), 6.06 (dd, J_{gem} = 2.39Hz; J_{trans} = 17.1Hz, 1H, **H$_b$**) , 5.54 (dd, J_{gem} = 2.39Hz; J_{cis} = 10.1Hz, 1H, **H$_a$**), 3.26 (m, 2H,–CH_2–C**H$_{e2}$**–NH–), 2.54 (t, $^2J_{H\text{-}H}$ = 7.7Hz, 2H,–**CH$_{f2}$**–CH_2–NH–).

Synthesis of PMMA by RAFT polymerization (PMMA-TTC). A typical polymerization of MMA was performed (Scheme 1 (2)) as follows: A round bottom flask was filled with MMA (10 g, 0.1 mol), 2-cyano-2-propyl dodecyl trithiocarbonate (CPDT, 69 mg, 1.9 10^{-4} mol), AIBN (6.5 mg, 3.99 10^{-5} mol) and toluene (2.3 mL). This mixture was placed in an ice bath at 0°C and degassed by Argon bubbling during 15min. The polymerization mixture was then heated at 70°C in a thermostated oil bath. Aliquots of the reaction mixtures were take-off, at different times and analyzed by ^{1}H NMR and GPC to estimate conversion (NMR spectra presented Figure S2 and Figure S3 respectively) and the molar masses of the PMMA formed during the reaction (SEC traces reported on Figure S4). The reaction mixture was then cooled down, open to the air and then poured into a large excess of cold methanol to precipitate the PMMA-TTC. The resulting polymer was then dried in a vacuum oven at 80°C overnight.

Synthesis of dopamine functionalized PMMA (PMMA-DA). The aminolysis and subsequent thia Michael addition were conducted using the one-pot protocol (Scheme 1 (3)) described by Guerre et al.[44] In a typical reaction, PMMA-TTC (M_n = 10,100 g mol^{-1}, 5g, 4.95 10^{-4} mol) and dopamine acrylamide (DA), (0.103 g, 5.00 10^{-4} mol) were dissolved in DMF (30 mL). The solution was degassed by argon bubbling for 10 min and a degassed mixture of n-butylamine (0.013 g, 1.83 10^{-4} mol) and DMPP (1.68 mg, 1.66 10^{-5} mol) in 1 mL of DMF was injected into the reaction mixture. Nitrogen bubbling was continued for a further 10 min and the reaction

solution was then stirred at 25 °C for 16 h. The pale-yellow solution was precipitated twice from chilled methanol, and the resulting white solid was recovered by centrifugation and dried under high vacuum at 50 °C until constant weight.

Synthesis of the BNT thin films. Firstly, a bottom electrode of $LaNiO_3$ (LNO) (200 nm) was sputtered on Si/SiO_2 substrate. Then lead-free $(Bi_{0.5}Na_{0.5})TiO_3$ (BNT) thin films (300 nm) were grown on Si/SiO_2/LNO by RF magnetron sputtering following a procedure previously described.[45] BNT was crystallized in perovskite structure with a (100) orientation enhanced by the structure matching between BNT and LNO, no second phase was observed. The obtained multilayer Si/SiO_2/LNO/BNT will be named BNT in the present study.

Preparation of BNT-PMMA. BNT thin films of $1cm^2$ were soaked into a solution of hydrogen peroxide (35 %vol) and then stirred at room temperature (25°C) for 24h. The thin films were further washed with H_2O and soaked in a solution of PMMA-DA (Mn = 10,100 g/mol, 10^{-3} M) in acetone/water (9:1 vol:vol). The reaction proceeded under stirring for 72h at room temperature (25°C). Then the thin films were washed with acetone using a sonicator bath to remove the ungrafted PMMA-DA chains.

Elaboration of BNT-PMMA/P(VDF-co-TrFE) bilayer composite. P(VDF-*co*-TrFE) powder was dissolved in acetone (20 mg/mL) and 0.4 mL of solution were spin-coated onto the BNT or BNT-PMMA substrates. The spinning speed and acceleration were respectively 2500 rpm and 3000 $m.s^{-2}$ for 45 seconds. The samples were then dried under a fume hood for 24h and further dried in a vacuum oven at 80°C for 4h.

RESULTS AND DISCUSSION

The aim of this study is to synthesize a catechol end-functionalized PMMA as a macromolecular coupling agent and to graft it onto a piezoelectric ceramic thin film (BNT) to improve the interfacial adhesion of a piezoelectric polymer P(VDF-*co*-TrFE) for piezoelectric

applications. For this purpose, PMMA was synthetized by RAFT using a trithiocarbonate as chain transfer agent (PMMA-TTC). The ω-end groups of the PMMA chains were functionalized with a dopamine acrylamide derivative (DA) via a one-pot aminolysis/thia Michael addition procedure and the resulting macromolecular coupling agent (PMMA-DA) was grafted onto the BNT surface. Finally, P(VDF-*co*-TrFE) was spin-coated on the modified BNT film and the crystalline domain of the copolymer as well as the local piezoelectric was investigated.

The synthesis of the dopamine acrylamide begins with an in-situ catechol protection step with borates. This procedure is well-known to prevent the self-polymerization of dopamine under basic conditions.[46,47,48] DA was obtained in relatively poor yield (32%) after column chromatography. This yield could be ascribed to the possible aza-michael addition which competed with the desired amide formation.

The RAFT polymerization of MMA (a more activated monomer (MAM)) is well controlled by trithiocarbonate RAFT agents featuring cyanopropyl R groups.[49–51] The polymerization of MMA was thus conducted using CPDT (2-cyano-2-propyl dodecyl trithiocarbonate) as chain transfer agent and a small amount of toluene as solvent to delay the massing of the polymerization mixture while keeping a high monomer concentration, increasing the polymerization rate and minimizing potential irreversible transfer to the solvent. Kinetics of the polymerization is depicted in Figure 1 and shows, as expected, a linear evolution of the molar masses (measured by SEC) with the conversion (calculated using ^{1}H NMR spectra reported in Figure S2 and S3) while the dispersity remained relatively low (below 1.3) during the entire polymerization, thus indicating the control of the polymerization. In addition, the synthesized polymers showed relatively symmetrical and narrow SEC traces (see Figure S4). In this study, the RAFT polymerization is not only used to produce well-defined polymer chains, but also to obtain functional ω-chain ends. Unfortunately, the overlapping of the resonance of the

backbone and the ω-chain end in ^{1}H NMR spectrum (Figure S3) prevented a clear estimation of the chain-end functionality of PMMA-TTC.

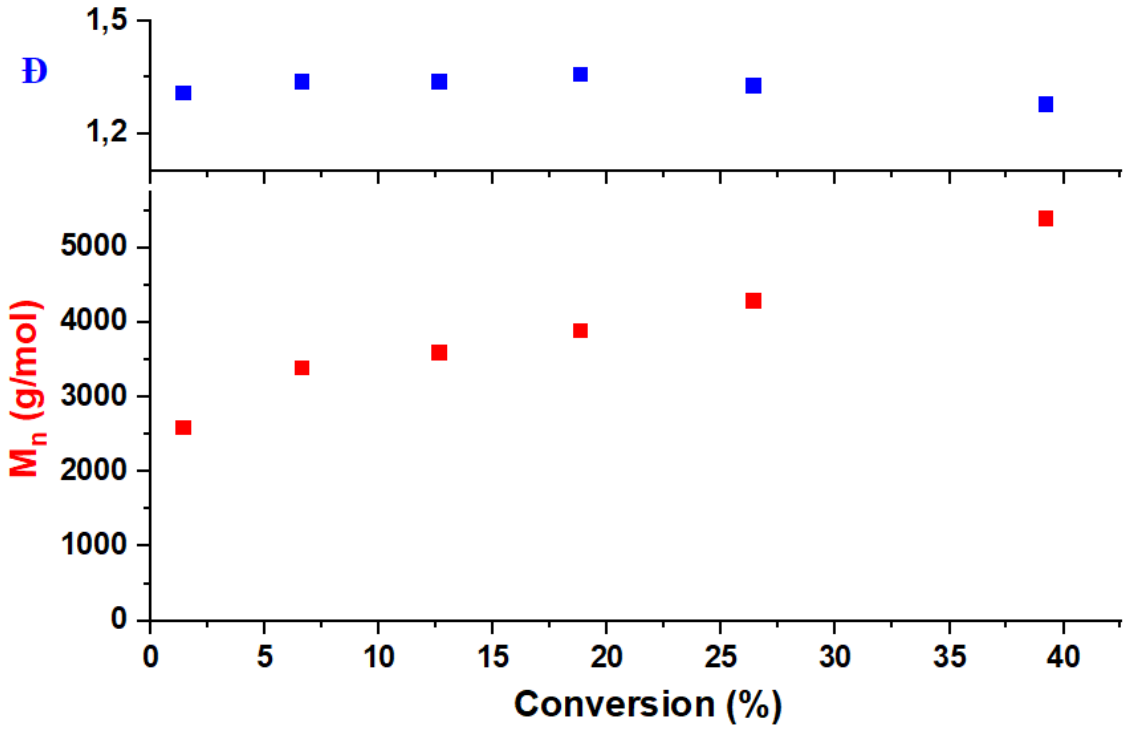

Figure 1. Evolution of the molar mass and dispersity of PMMA with conversion during the RAFT polymerization of MMA using CPDT as transfer agent. [MMA]:[TTC]:[AIBN] = 100:1:0.1, Temp = 70°C, reaction time = 9h, See Table S1.

The synthesis of the PMMA-DA polymer consists in a one-pot two step reaction allowing the substitution of the functional RAFT chain-end with a catechol moiety possessing adhesive properties.

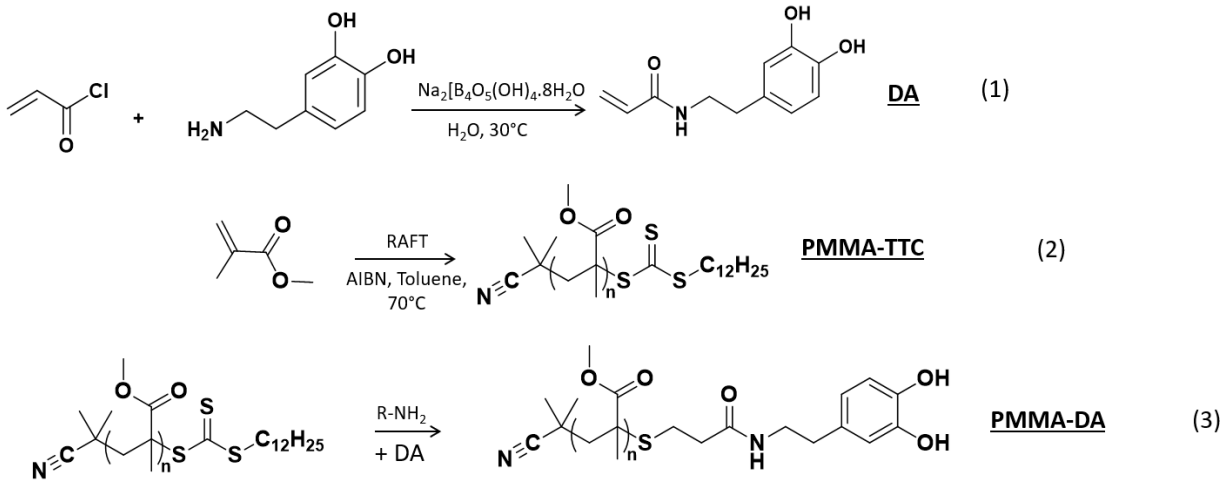

Scheme 1. Reaction scheme of the synthesis of the PMMA-DA coupling agent.

Briefly, *N*-butylamine was used as nucleophile to convert the thiocarbonylthio group into thiol while DMPP was used as a catalyst.[44] This catalytic effect has been studied by Bowman et al.[52] Afterwards, DA was employed as a Michael acceptor to introduce the catechol moiety at the PMMA chain-end via thiol-ene addition. Indeed, McKee et al.[53] showed previously that the aminolysis and the thia-Michael addition were faster than the aza-Michael addition thus allowing the generated thiol to readily react with the acrylamide.

The successful anchoring of the catechol unit at the ω-chain end of the PMMA was evidenced by recording ^{1}H NMR spectrum (Figure 2) which exhibited typical resonances of the catechol moiety between 6.5 and 6.75 ppm. Using the DP values calculated from the SEC analyses (using PMMA standards and thus, giving true molar masses) and the integration of the resonances of the polymer backbone (resonance of the methylene group at 3.6ppm) and of the catechol group, a functionalization of 70% of chain end was estimated.

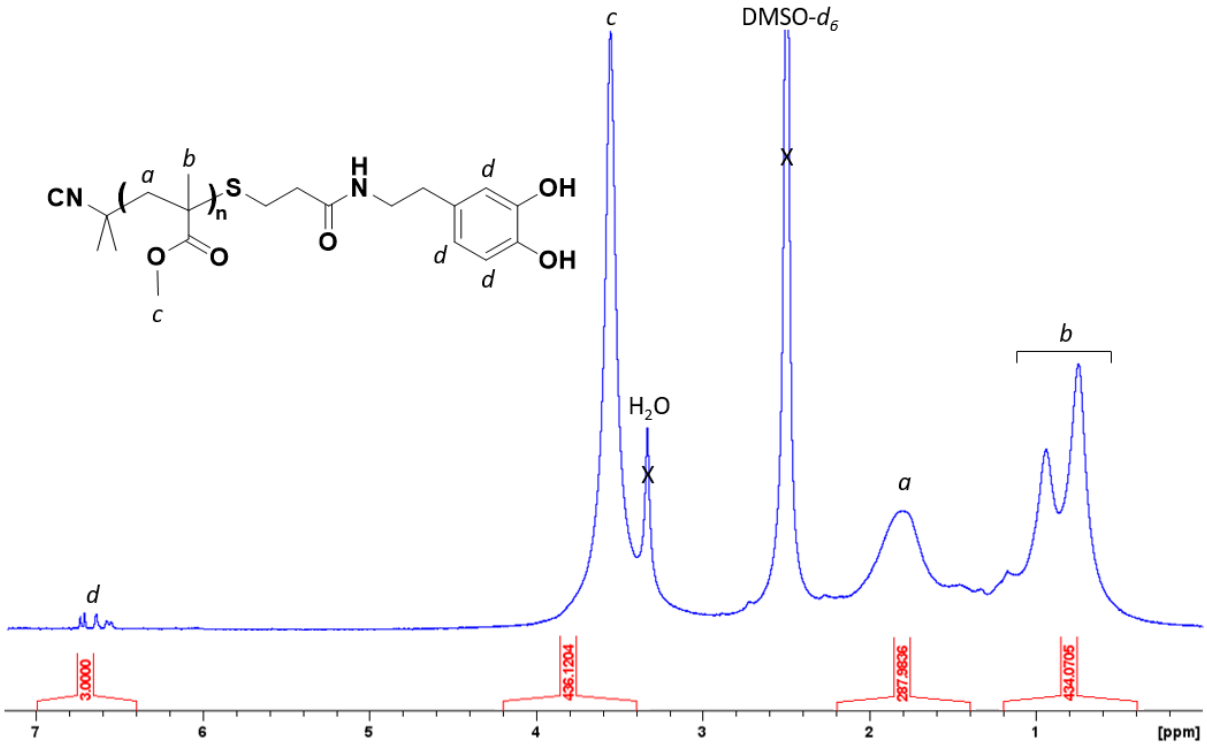

Figure 2. ^{1}H NMR spectrum in DMSO-d_6 of the PMMA-DA prepared by chain-end modification of PMMA-TTC (Entry 1, Table S1).

Finally, the presence of the catechol moiety in the polymer chains was further evidenced by cyclic voltammetry (CV) (Figure 3). Indeed, the CV of the dopamine end-functionalized polymers gave rise to the irreversible two-electron oxidation wave around 1.1V vs Ag/AgCl, corresponding to the two-step oxidation of the catechol unit as observed for the Dopamine-Acrylamide derivative.

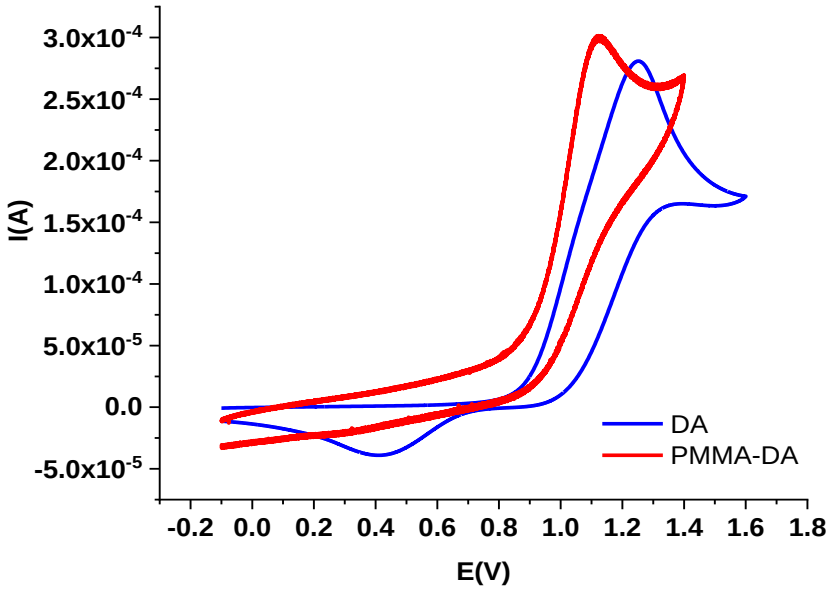

Figure 3. Cyclic voltammograms (CV) of Dopamine-Acrylamide (DA) and PMMA-DA in acetonitrile (Entry 8, Table S1). The intensity of the PMMA-DA was increased by 15. CV were recorded at $C=2.10^{-4}M^{-1}$ in the presence of Bu_4NPF_6 (0.05M). Platinum working electrode; Ag/AgCl reference electrode. Scan rate of 50 $mV.s^{-1}$.

Prior to the grafting of the PMMA-DA (Mn = 10,100 g/mol) , the BNT surface was activated using the protocol described by Gao et al.[54] in order to promote the formation of hydroxylated groups at the surface of the BNT films thus enhancing the grafting of the catechol units. Briefly, the BNT samples were soaked into a hydrogen peroxide solution at 30% for 24h. After washing, the macromolecular coupling agent PMMA-DA was grafted onto the activated BNT surface (BNT-OH, Scheme 2). For this purpose, the activated films (labelled BNT-OH) were soaked into a solution of PMMA-DA (10^{-3}M). The coated BNT wafers (labelled BNT-PMMA, Scheme 2) were then rinsed with acetone to remove the ungrafted chains and then sonicated for 5 minutes in acetone. Afterwards, the ability of the macromolecular coupling agent to graft onto the piezoelectric film surface was then examined by using water contact angle measurements

(Table S2). First, the treatment with hydrogen peroxide significantly modified the BNT surface, making it more hydrophilic with a water contact angle (WCA) decreasing from 70.2 ± 2.4° to 44.8 ± 3.2° in accordance with the generation of hydroxylated groups onto the BNT surface. In contrast, the BNT surface became more hydrophobic after PMMA-DA grafting as the WCA increased from 44.8 ± 3.2° to 58.3 ± 2.7°. This result is in relatively good agreement with the WCA values of 68° reported for a film of PMMA.[55] Additional contact angle measurements were carried out with diiodomethane and formamide (Table S2) providing the means to calculate the energy of the BNT wafers surface after the different treatments. This surface energy (calculated using the OWRK method using equation S1) follows the same trend as the WCA, increasing with the hydrogen peroxide activation and decreasing slightly upon deposition of the PMMA-DA to reach 44.9 mN/m, a value close to that reported for PMMA surfaces (41.1 mN/m).[55,56] These results confirm the effectiveness of the PMMA-DA grafting on BNT.

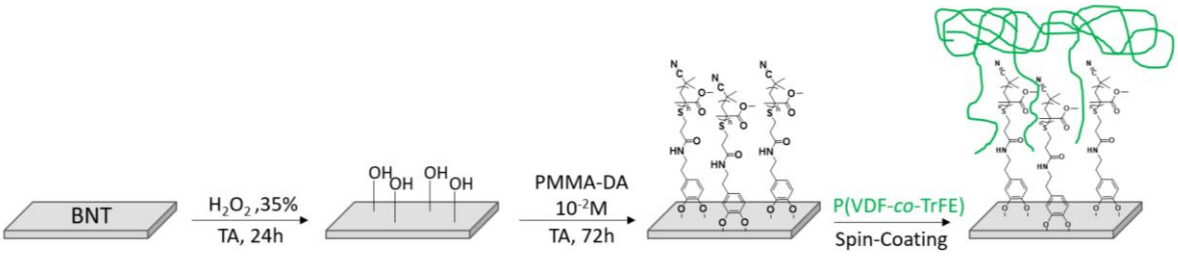

Scheme 2. Elaboration of the BNT-PMMA/P(VDF-*co*-TrFE) bilayer composite.

The bilayer composites were elaborated by adding copolymer by spin coating onto the raw BNT and the modified BNT-PMMA as presented on Scheme 2. The cross section of BNT-PMMA/P(VDF-*co*-TrFE) composites analyzed by SEM-EDX is presented in Figure 4 and Figure S5. The images allow the identification of the different inorganic and polymer layers. From left to right, these EDX images show the presence of silicon (Si) due to the SiO_2 wafer (few micrometers), of nickel (Ni) characteristic of the LNO layer (200 nm), of bismuth (Bi) and

sodium (Na) corresponding to the BNT (300 nm), and finally of fluorine (F) in the outer layer indicating the presence of the fluoropolymer (300-400 nm). Nevertheless, the PMMA layer is too thin (less than 3-4 nm, the limit of resolution of the SEM images) to be observed and does not possess elements that facilitate EDX observations (no signal for sulphur or nitrogen).

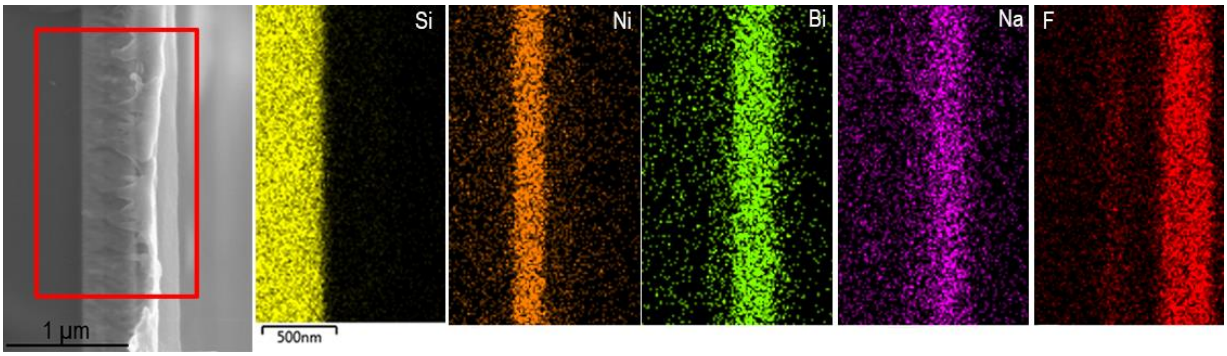

Figure 4. SEM images and associated EDX maps of the cryofractured Si/SiO_2/LNO/BNT-PMMA/P(VDF-*co*-TrFE) composite recorded at 5kV. The estimated thicknesses of the LNO, BNT and P(VDF-*co*-TrFE) layers are 200 nm, 300 nm and 350 nm, respectively.

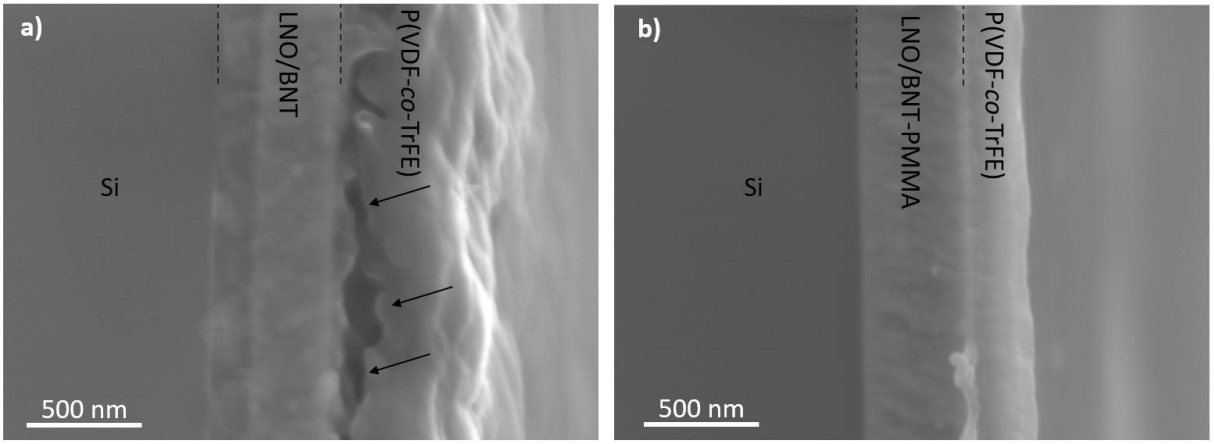

Figure 5. SEM images of bilayer composite cryofracture for P(VDF-*co*-TrFE) on a) untreated BNT and b) BNT-PMMA substrates.

SEM images for the cryofractured composite bilayer of P(VDF-*co*-TrFE) onto untreated BNT and BNT-PMMA are presented in Figure 5. The cryofracture step requires the composite immersion in liquid nitrogen which induces a contraction of the polymer layer. This contraction causes stress and, in the case of untreated BNT, leads to the presence of cavities at the interface between fluoropolymer and ceramic (black arrows in Figure 5a). In contrast, the cavities are not observed in the composite prepared from BNT-PMMA (Figure 5b). In spite of the cryofracture step, the BNT-PMMA/P(VDF-*co*-TrFE) interface remained cohesive. This result clearly indicates that the addition of the PMMA-DA coupling agent enhanced the adhesion between the ceramic and the polymer materials and demonstrates the efficiency of PMMA-DA as coupling agent to improve interfacial adhesion in BNT/fluoropolymer composite.

To study the impact of the PMMA-DA coupling agent on the copolymer crystal structure and on the orientation of macromolecular chains, GIWAXS measurements were performed on the fluoropolymer layer deposited on the untreated BNT and on the BNT-PMMA. The GIWAXS patterns shows the presence of one main discontinuous ring characteristic of a non-isotropic repartition of the crystalline lamellae (Figure 6a). The integrated intensity profile of both samples shows the presence of a main peak at $2\theta = 19.9°$ associated to the (200)/(110) planes (Figure 6b) and attributed to the polar P(VDF-*co*-TrFE) ferroelectric (FE) phase (sometimes called β-phase by analogy with PVDF). The interplanar distances are characteristic of an orthorhombic unit cell with the parameters a = 0.890 nm, b = 0.505 nm and c = 0.255 nm.[57]

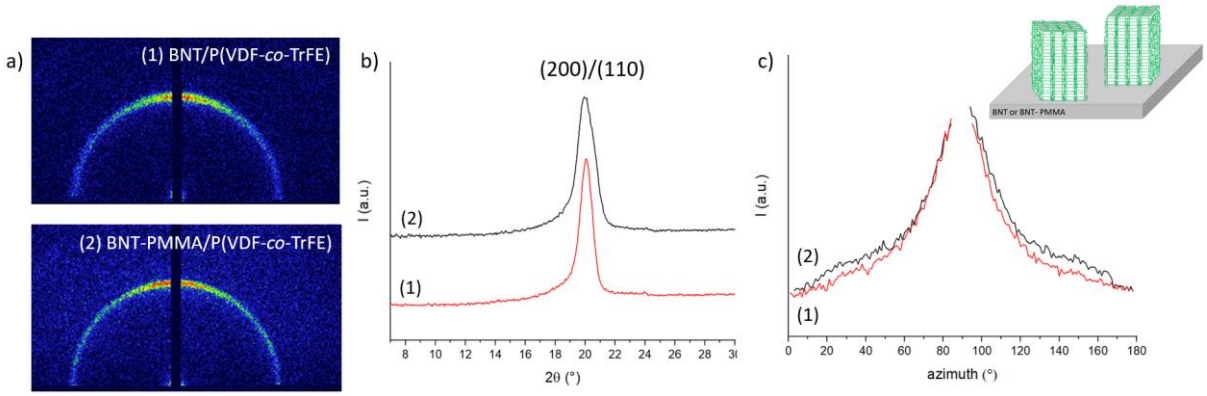

Figure 6. a) GIWAXS patterns of P(VDF-*co*-TrFE) copolymer layer on (1) untreated BNT and (2) BNT-PMMA, b) integrated intensity profiles and c) azimuth intensity profiles of (200)/(110) crystalline reflections, the inset shows the simplified schematic representation of crystalline lamellas orientation of P(VDF-*co*-TrFE) on the BNT or BNT-PMMA substrate.

The presence of PMMA miscible with the copolymer has no significant influence on the P(VDF-*co*-TrFE) crystal phase. The position of the diffraction peak is not impacted indicating no change in the copolymer unit cell and the normalized intensity are pretty similar. These results are in accordance with the small amount of miscible polymer blended with the copolymer. It is interesting to note that the copolymer crystal phase adopted a particular orientation on the substrates. To analyze this orientation, the azimuthal profile of the main (200)/(110) reflection is reported in Figure 6c. The profile clearly shows an intense reflections on the meridian ($90 \pm 2°$) which is consistent with the orientation of the macromolecular chains, along the crystallographic c-axis, parallel to the substrate[58] and the orientation of crystalline lamellae perpendicular to the substrate surface (as schematically presented in the inset of Figure 6c). Therefore, the polarization vector oriented along the b-axis[59] may give, under the application of an external electrical field, a high ferroelectric response as investigated by Park et al.[60] on similar P(VDF-*co*-TrFE) copolymer.

The surface morphology of the P(VDF-*co*-TrFE) layer deposited onto BNT-PMMA was characterized by TM-AFM. Clear disordered rice-like grains were observed (Figure 7a) with average lateral dimensions of 150 nm (in length) and 80 nm (in width). Such nanometric structures correspond to P(VDF-*co*-TrFE) crystalline domains. From the TM-AFM amplitude error signal shown on Figure 7b, crystalline lamellae separated by amorphous interlamellar regions can be distinguished, as recently well-evidenced by J. Hafner et al.[61] The cross-section profile of the amplitude error signal through a rice-like grain (corresponding to the dashed yellow line in Figure 7b) is presented in Figure 7c and highlights more precisely the arrangement of crystalline and amorphous regions with a stack of lamellae perpendicular to the substrate. The average thickness of the lamellae was determined at about 4-7 nm and the distance between two crystalline lamellae separated by amorphous phase was about 8 nm, in agreement with values already published.[61,62] The presence of the PMMA did not prevent the formation of the typical surface morphology of the P(VDF-*co*-TrFE) polar ferroelectric phase.

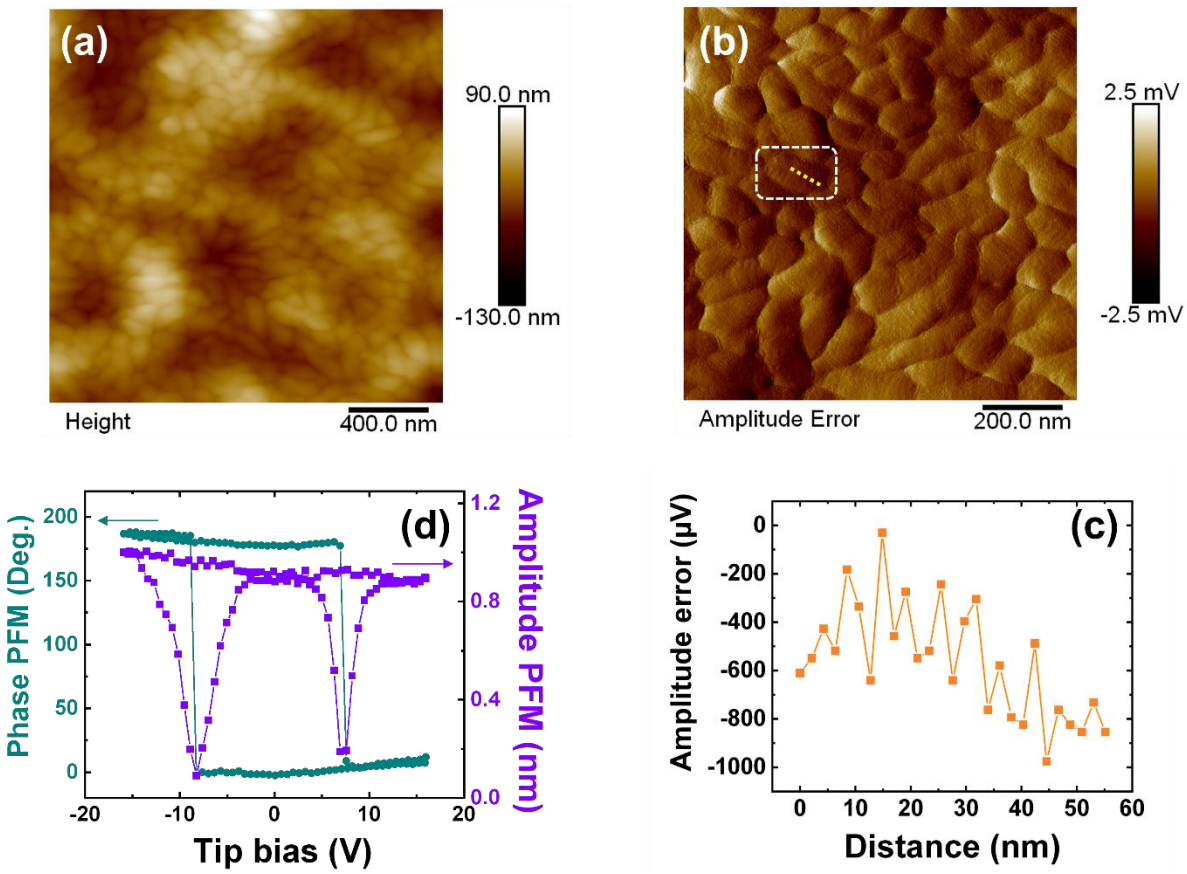

Figure 7. TM-AFM (a) height and (b) amplitude error images recorded at the surface of the P(VDF-*co*-TrFE) layer when deposited onto BNT-PMMA. (c) Amplitude error profile corresponding to the dashed yellow line through a rice-like grain highlighted in (b). (d) Typical remnant phase and amplitude PFM loops measured at the center of the rice-like grains of the P(VDF-*co*-TrFE) film.

The electroactive behavior of the copolymer layer was then investigated by measuring remnant (off-field) PFM hysteresis loops over the free surface. For that, the nanometric probing tip was positioned in the center of the rice-like grain, while a pulsed triangular DC bias sequence superimposed on the AC driving voltage was applied. Typical out-of-plane phase and amplitude PFM loops were obtained (Figure 7d). Square hysteresis response was obtained from the phase signal, revealing the two opposite polarization states expected for such local polarization reversal experiments. An average coercive voltage of 7.7 V was determined, leading to a

coercive field of about 31 MV/m. The amplitude signal shows well-defined butterfly shape, in agreement with the inverse piezoelectric effect occurring under such electrical stimuli. From the maximum deformation amplitude detected and considering a quality factor of about 54,[62] an effective piezoelectric coefficient of –18.5 pm/V was estimated.

In addition, as-grown out-of-plane PFM response was observed over the surface of the BNT-PMMA/P(VDF-*co*-TrFE) bilayer, as shown in Figure S6. The strong contrasts observed on both phase and amplitude PFM patterns further support the clear piezo-/ferroelectric nature of the copolymer layer.

The local out-of-plane piezo-activity detected from spectroscopic or imaging PFM modes is in perfect agreement with the specific orientation of the polarization vector which is, here, directed perpendicular to the surface. In this case, the $–CF_2–$ dipole moments can easily rotate around the horizontal c-axis under application of out-of-plane electric field.[63] Consequently, the PFM-based analysis shows the electroactive behavior of the P(VDF-*co*-TrFE) layer, related to the rice-like crystalline grains, in the presence of PMMA. This result evidences the usefulness of the PMMA as a coupling agent while preserving the polar phase of the fluoropolymer, which is essential for the development of piezoelectric ceramic/polymer composites.

CONCLUSIONS

Catechol end-functionalized PMMA with relative low dispersity were successfully synthesized by RAFT polymerization and subsequent one pot aminolysis / thia-Michael addition using dopamine acrylamide as Michael acceptor. The presence of the catechol unit at the chain end was confirmed using cyclic voltammetry and NMR measurements. The ratio of PMMA chains featuring a catechol groups at the chain end (PMMA-DA) was around 70%. BNT thin films were oxidized using hydrogen peroxide to promote the grafting of the PMMA-DA and the surface modification was confirmed using contact angle measurements. Then,

piezoelectric bilayers composites were fabricated by depositing a P(VDF-*co*-TrFE) layer of around 300 nm onto the BNT and PMMA-modified BNT. The interfacial adhesion of cryofractured bilayers was compared by SEM observations on the edge of the composite. Several cavities and delamination of the fluoropolymer layer were observed for the composite prepared from the unmodified BNT while the fluoropolymer and the BNT-PMMA showed a strong cohesive interface. Further, GIWAXS measurements were carried out to confirm that the additional PMMA layer was not affecting the crystalline properties of the P(VDF-*co*-TrFE). Finally, typical nanometric rice-like grains were observed on the polymer surface, and were associated to strong local electroactive properties, as revealed by AFM and PFM analyses. This study proves that the use of the PMMA-DA coupling agent has beneficial effect for ceramic/polymer piezoelectric composites by strengthening the interfacial cohesion. This study paves the way for a better understanding of the effect of the coupling agents in piezoelectric composites.

ASSOCIATED CONTENT

Supporting Information.

The Supporting Information is available. Table S1 (MMA RAFT polymerization data), Table S2 (Contact angle measurements), Equation S1 (Surface energy calculations), Figure S1 (^{1}H NMR of Dopamine-Acrylamide), Figure S2 (^{1}H NMR of crude PMMA-TTC), Figure S3 (^{1}H NMR monitoring of the RAFT polymerization of MMA), Figure S4 (SEC monitoring of the RAFT polymerization of MMA), Figure S5 (SEM-EDX of the bilayer composite), Figure S6 (AFM and PFM analyses).

AUTHOR INFORMATION

Corresponding Authors

*E-mail: sophie.barrau@univ-lille.fr

*E-mail: vincent.ladmiral@enscm.fr

Author Contributions

The manuscript was written through contributions of all authors. All authors have given approval to the final version of the manuscript.

Funding Sources

This work was supported by the French National Research Agency (NanoPiC grant, ANR-16-CE08-0025).

ACKNOWLEDGMENTS

The authors thank Arkema (Pierre-Bénite, France) for providing P(VDF-co-TrFE). This work was carried out on the Electron Microscopy Facility and on the X-Ray Diffraction and Diffusion Facility of the Advanced Characterization Platform of the Chevreul Institute. The authors gratefully acknowledge the Chevreul Institute, Ministère de l'Enseignement Supérieur, de la Recherche et de l'Innovation, Hauts-de-France Region, Fonds Européen de Développement Régional (FEDER), and Major Domain of Interest (DIM) "Eco-Energy Efficiency" of Artois University for equipment in particular the MFP-3D microscope made available for performing experiments.

REFERENCES

(1) Ihlefeld, J. F. Fundamentals of Ferroelectric and Piezoelectric Properties. *Ferroelectricity in Doped Hafnium Oxide: Materials, Properties and Devices; Elsevier* **2019**, 1–24.

(2) Ribeiro, C.; Costa, C. M.; Martins, P.; Correia, V.; Lanceros-Mendez, S. Piezoelectric Polymers and Polymer Composites for Sensors and Actuators. *Reference Module in Materials Science and Materials Engineering; Elsevier* **2018**, 1–11.

(3) Chorsi, M. T.; Curry, E. J.; Chorsi, H. T.; Das, R.; Baroody, J.; Purohit, P. K.; Ilies, H.; Nguyen, T. D. Piezoelectric Biomaterials for Sensors and Actuators. *Adv. Mater.* **2019**, *31* (1), 1–15.

(4) van der Zwaag, S.; van den Ende, D. A.; Groen, W. A. (Pim). Sensing and Energy Harvesting Novel Polymer Composites. *Materials Experience; Elsevier* **2014**; 221–234.

(5) Lynch, C. S.; Liao, X.; Cochran, S. The Performance of Piezoelectric Materials Under Stress. *Advanced Piezoelectric Materials; Elsevier* **2017**; 787–814.

(6) Malič, B.; Kuščer, D.; Vrabelj, M.; Koruza, J. Review of Methods for Powder-Based Processing. *Magnetic, Ferroelectric, and Multiferroic Metal Oxides; Elsevier* **2018**; 95–120.

(7) Hooker, W. Properties Ceramics of PZT-Based Piezoelectric and 250 ° C. *NASA Langley Tech. Rep. Serv.* **1998**.

(8) Wang, K.; Li, J.-F. (K, Na)NbO3-Based Lead-Free Piezoceramics: Phase Transition, Sintering and Property Enhancement. *J. Adv. Ceram.* **2012**, *1* (1), 24–37.

(9) Shen, Z. Y.; Li, J. F. Enhancement of Piezoelectric Constant D_{33} in $BaTiO_3$ Ceramics Due to Nano-Domain Structure. *J. Ceram. Soc. Japan* **2010**, *118* (1382), 940–943.

(10) Takenaka T. Nagata H., Sodium Bismuth Titanate based Ceramics. *Lead-Free Piezoelectrics; Elsevier* **2012**; 255-290.

(11) Takenaka, T. Lead-Free Piezo-Ceramics. *Adv. Piezoelectric Mater. Sci. Technol.* **2010**, 130–170.

(12) Kim, H. P.; Ahn, C. W.; Hwang, Y.; Lee, H. Y.; Jo, W. Strategies of a Potential Importance, Making Lead-Free Piezoceramics Truly Alternative to PZTs. *J. Korean Ceram. Soc.* **2017**, *54* (2), 86–95.

(13) Nie, H.; Wang, G.; Dong, X. New Bismuth Sodium Titanate Based Ceramics and Their Applications. *Advanced Ceramic Materials*; **2021**.

(14) Rödel, J.; Webber, K. G.; Dittmer, R.; Jo, W.; Kimura, M.; Damjanovic, D. Transferring Lead-Free Piezoelectric Ceramics into Application. *J. Eur. Ceram. Soc.* **2015**, *35* (6), 1659–1681.

(15) Yamada, T.; Ueda, T.; Kitayama, T. Piezoelectricity of a High-Content Lead Zirconate Titanate/Polymer Composite. *J. Appl. Phys.* **1982**, *53* (6), 4328–4332.

(16) Lang, S. B.; Muensit, S. Review of Some Lesser-Known Applications of Piezoelectric and Pyroelectric Polymers. *Appl. Phys. A Mater. Sci. Process.* **2006**, *85* (2), 125–134.

(17) Fukada, E. Recent Developments of Polar Piezoelectric Polymers. *IEEE Trans. Dielectr. Electr. Insul.* **2006**, *13* (5), 1110–1119.

(18) Bauer, S.; Bauer, F. Piezoelectric Polymers and Their Applications. *Springer Ser. Mater. Sci.* **2008**, *114*, 157–177.

(19) Hasegawa, R.; Takahashi, Y.; Chatani, Y.; Tadokoro, H. Crystal Structures of Three Crystalline Forms of Poly(Vinylidene Fluoride). *Polym. J.* **1972**, *3* (5), 600–610.

(20) Kobayashi, M.; Tashiro, K.; Tadokoro, H. Molecular Vibrations of Three Crystal Forms of Poly(Vinylidene Fluoride). *Macromolecules* **1975**, *8* (2), 158–171.

(21) Crecorio, R.; Cestari, M. Effect of Temperature on the Crystalline Phase Content and Morphology of Poly (Vinylidene Fluoride). *J. Polym. Sci., Part B: Polym. Phys.* **2006**, *32*, 859–870.

(22) Sencadas, V.; Moreira, V. M.; Lanceros-Mendéz, S.; Pouzada, A. S.; Gregório, R. α - To - β Transformation on PVDF Films Obtained by Uniaxial Stretch. *Mater. Sci. Forum* **2006**, *514–516* (PART 2), 872–876.

(23) Defebvin, J.; Barrau, S.; Stoclet, G.; Rochas, C.; Lefebvre, J. M. In Situ SAXS/WAXS Investigation of the Structural Evolution of Poly(Vinylidene Fluoride) upon Uniaxial Stretching. *Polymer* **2016**, *84*, 148–157.

(24) Oka, Y.; Koizumi, N. Formation of Unoriented Form I Poly (Vinylidene Fluoride) by High-Rate Quenching and Its Electrical Properties (Commemoration Issue Dedicated to Professor Naokazu Koizumi on the Occasion of His Retirement). *Bull. Inst. Chem. Res., Kyoto Univ.* **1985**, *63*, 192–206.

(25) Weinhold, S.; Litt, M. H.; Lando, J. B. The Crystal Structure of the γ Phase of Poly(Vinylidene Fluoride). *Macromolecules* **1980**, *13* (5), 1178–1183.

(26) Sencadas, V.; Gregorio Filho, R.; Lanceros-Mendez, S. Processing and Characterization of a Novel Nonporous Poly(Vinilidene Fluoride) Films in the β Phase. *J. Non. Cryst. Solids* **2006**, *352* (21–22), 2226–2229.

(27) Jia, N.; He, Q.; Sun, J.; Xia, G.; Song, R. Crystallization Behavior and Electroactive Properties of PVDF, P(VDF-TrFE) and Their Blend Films. *Polym. Test.* **2017**, *57*, 302–306.

(28) Bargain, F.; Panine, P.; Domingues Dos Santos, F.; Tencé-Girault, S. From Solvent-Cast to Annealed and Poled Poly(VDF-Co-TrFE) Films: New Insights on the Defective Ferroelectric Phase. *Polymer* **2016**, *105*, 144–156.

(29) Greeshma, T.; Balaji, R.; Jayakumar, S. PVDF Phase Formation and Its Influence on Electrical and Structural Properties of PZT-PVDF Composites. *Ferroelectr., Lett. Sect.* **2013**, *40* (1–3), 41–55.

(30) Lam, K. H.; Chan, H. L. W. Piezoelectric and Pyroelectric Properties of 65PMN-

35PT/P(VDF-TrFE) 0-3 Composites. *Compos. Sci. Technol.* **2005**, *65* (7–8), 1107–1111.

(31) Ploss, B.; Ploss, B.; Shin, F. G.; Chan, H. L. W.; Choy, C. L. Pyroelectric or Piezoelectric Compensated Ferroelectric Composites. *Appl. Phys. Lett.* **2000**, *76* (19), 2776–2778.

(32) Yang, K.; Huang, X.; Huang, Y.; Xie, L.; Jiang, P. Fluoro-Polymer@BaTiO3 Hybrid Nanoparticles Prepared via RAFT Polymerization: Toward Ferroelectric Polymer Nanocomposites with High Dielectric Constant and Low Dielectric Loss for Energy Storage Application. *Chem. Mater.* **2013**, *25* (11), 2327–2338.

(33) A. Safari. Development of piezoelectric composites for transducers. *Journal de Physique III, EDP Sciences*, **1994**, 4 (7), 1129-1149.

(34) Saiz-Poseu, J.; Mancebo-Aracil, J.; Nador, F.; Busqué, F.; Ruiz-Molina, D. The Chemistry behind Catechol-Based Adhesion. *Angew. Chemie - Int. Ed.* **2019**, *58* (3), 696–714.

(35) Defebvin, J.; Barrau, S.; Lyskawa, J.; Woisel, P.; Lefebvre, J. M. Influence of Nitrodopamine-Functionalized Barium Titanate Content on the Piezoelectric Response of Poly(Vinylidene Fluoride) Based Polymer-Ceramic Composites. *Compos. Sci. Technol.* **2017**, *147*, 16–21.

(36) Mayeen, A.; Kala, M. S.; Jayalakshmy, M. S.; Thomas, S.; Rouxel, D.; Philip, J.; Bhowmik, R. N.; Kalarikkal, N. Dopamine Functionalization of BaTiO3: An Effective Strategy for the Enhancement of Electrical, Magnetoelectric and Thermal Properties of BaTiO3-PVDF-TrFE Nanocomposites. *Dalt. Trans.* **2018**, *47* (6), 2039–2051.

(37) Mitharwal, C.; Geetanjali; Malhotra, S.; Bagla, A.; Srivastava, M. K.; Gupta, S. M.; Negi, C. M. S.; Kar, E.; Kulkarni, A. R.; Mitra, S. Performance of Dopamine Modified 0.5(Ba0.7Ca0.3)TiO3-0.5Ba(Zr0.2Ti0.8)O3 Filler in PVDF Nanocomposite as Flexible Energy Storage and Harvester. *J. Alloys Compd.* **2021**, *876*, 160141.

(38) Pimbert, S.; Avignon-Poquillon, L.; Levesque, G. Calorimetric Study of Fluorinated

Methacrylic and Vinyl Polymer Blends: Part 2: Correlation between Miscibility, Chemical Structure and χ 12 Interaction Parameter in Binary Systems. *Polymer* **2002**, *43* (11), 3295–3302.

(39) Mijovic, J.; Sy, J.-W.; Kwei, T. K. Reorientational Dynamics of Dipoles in Poly(Vinylidene Fluoride)/Poly(Methyl Methacrylate) (PVDF/PMMA) Blends by Dielectric Spectroscopy. *Macromolecules* **1997**, *30* (10), 3042–3050.

(40) Schneider, S.; Drujon, X.; Wittmann, J. C.; Lotz, B. Impact of Nucleating Agents of PVDF on the Crystallization of PVDF/PMMA Blends. *Polymer* **2001**, *42* (21), 8799–8806.

(41) Owens, D. K.; Wendt, R. C. Estimation of the Surface Free Energy of Polymers. *J. Appl. Polym. Sci.* **1969**, *13*, 1741–1747.

(42) Rodriguez, B. J.; Callahan, C.; Kalinin, S. V.; Proksch, R. Dual-Frequency Resonance-Tracking Atomic Force Microscopy. *Nanotechnology* **2007**, *18* (47), 475504.

(43) Patil, N.; Falentin-Daudré, C.; Jérôme, C.; Detrembleur, C. Mussel-Inspired Protein-Repelling Ambivalent Block Copolymers: Controlled Synthesis and Characterization. *Polym. Chem.* **2015**, *6* (15), 2919–2933.

(44) Guerre, M.; Ladmiral, V. One-Pot Synthesis of Poly (Vinylidene Fluoride) Methacrylate Macromonomer via Thia - Michael Addition. *Polym. Chem.* **2016**, 7, 441–450.

(45) Hamieh, A.; Ponchel, F.; Barrau, S.; Remiens, D. Synthesis of Lead-Free $(Bi_{0,5}Na_{0,5})TiO_3$ Thin Film by RF Magnetron Sputtering: Impact of Na on the Properties of Film. *Ferroelectrics* **2020**, *556*, 79-86.

(46) Liu, Y.; Ai, K.; Lu, L. Polydopamine and Its Derivative Materials: Synthesis and Promising Applications in Energy, Environmental, and Biomedical Fields. *Chem. Rev.* **2014**, *114* (9), 5057–5115.

(47) Maon, L. Mussel-Inspired Surface Chemistry for Multifunctional Coatings. *J. Chem. Inf.*

Model. **2013**, *53* (9), 1689–1699.

(48) Lee, B. P.; Huang, K.; Nunalee, F. N.; Shull, K. R.; Messersmith, P. B. Synthesis of 3,4-Dihydroxyphenylalanine (DOPA) Containing Monomers and Their Co-Polymerization with PEG-Diacrylate to Form Hydrogels. *J. Biomater. Sci. Polym. Ed.* **2004**, *15* (4), 449–464.

(49) Moad, G.; Chong, Y. K.; Postma, A.; Rizzardo, E.; Thang, S. H. Advances in RAFT Polymerization: The Synthesis of Polymers with Defined End-Groups. *Polymer* **2005**, *46* (19), 8458–8468.

(50) Parkatzidis, K.; Truong, N. P.; Antonopoulou, M. N.; Whitfield, R.; Konkolewicz, D.; Anastasaki, A. Tailoring Polymer Dispersity by Mixing Chain Transfer Agents in PET-RAFT Polymerization. *Polym. Chem.* **2020**, *11* (31), 4968–4972.

(51) Hummel, P.; Lechner, A. M.; Herrmann, K.; Biehl, P.; Rössel, C.; Wiedenhöft, L.; Schacher, F. H.; Retsch, M. Thermal Transport in Ampholytic Polymers: The Role of Hydrogen Bonding and Water Uptake. *Macromolecules* **2020**, *53* (13), 5528–5537.

(52) Chan, J. W.; Hoyle, C. E.; Lowe, A. B.; Bowman, M. Nucleophile-Initiated Thiol-Michael Reactions: Effect of Organocatalyst, Thiol, and Ene. *Macromolecules* **2010**, *43* (15), 6381–6388.

(53) McKee, J. R.; Ladmiral, V.; Niskanen, J.; Tenhu, H.; Armes, S. P. Synthesis of Sterically-Stabilized Polystyrene Latexes Using Well-Defined Thermoresponsive Poly(N-Isopropylacrylamide) Macromonomers. *Macromolecules* **2011**, *44* (19), 7692–7703.

(54) Gao, L.; He, J.; Hu, J.; Li, Y. Large Enhancement in Polarization Response and Energy Storage Properties of Poly(Vinylidene Fluoride) by Improving the Interface Effect in Nanocomposites. *J. Phys. Chem. C* **2014**, *118* (2), 831–838.

(55) Ma, Y.; Cao, X.; Feng, X.; Ma, Y.; Zou, H. Fabrication of Super-Hydrophobic Film from

PMMA with Intrinsic Water Contact Angle below 90°. *Polymer* **2007**, *48* (26), 7455–7460.

(56) Solid-Surface-Energy @ Www.Surface-Tension.De.

(57) Bellet-Amalric, E.; Legrand, J. F. Crystalline Structures and Phase Transition of the Ferroelectric P(VDF-TrFE) Copolymers, a Neutron Diffraction Study. *Eur. Phys. J. B* **1998**, *3* (2), 225–236.

(58) Spampinato, N.; Maiz, J.; Portale, G.; Maglione, M.; Hadziioannou, G.; Pavlopoulou, E. Enhancing the Ferroelectric Performance of P(VDF-Co-TrFE) through Modulation of Crystallinity and Polymorphism. *Polymer* **2018**, *149*, 66–72.

(59) Hu, Z.; Tian, M.; Nysten, B.; Jonas, A. M. Regular Arrays of Highly Ordered Ferroelectric Polymer Nanostructures for Non-Volatile Low-Voltage Memories. *Nat. Mater.* **2009**, *8* (1), 62–67.

(60) Park, Y. J.; Kang, S. J.; Park, C.; Kim, K. J.; Lee, H. S.; Lee, M. S.; Chung, U.-I.; Park, I. J. Irreversible Extinction of Ferroelectric Polarization in P(VDF-TrFE) Thin Films upon Melting and Recrystallization. *Appl. Phys. Lett.* **2006**, *88* (24), 242908.

(61) Hafner, J.; Benaglia, S.; Richheimer, F.; Teuschel, M.; Maier, F. J.; Werner, A.; Wood, S.; Platz, D.; Schneider, M.; Hradil, K.; Castro, F. A.; Garcia, R.; Schmid, U. Multi-Scale Characterisation of a Ferroelectric Polymer Reveals the Emergence of a Morphological Phase Transition Driven by Temperature. *Nat. Commun.* **2021**, *12* (1), 152.

(62) Katsouras, I.; Asadi, K.; Li, M.; Van Driel, T. B.; Kjær, K. S.; Zhao, D.; Lenz, T.; Gu, Y.; Blom, P. W. M.; Damjanovic, D.; Nielsen, M. M.; De Leeuw, D. M. The Negative Piezoelectric Effect of the Ferroelectric Polymer Poly(Vinylidene Fluoride). *Nat. Mater.* **2016**, *15* (1), 78–84.

(63) Hu, W. J.; Juo, D. M.; You, L.; Wang, J.; Chen, Y. C.; Chu, Y. H.; Wu, T. Universal Ferroelectric Switching Dynamics of Vinylidene Fluoride-Trifluoroethylene Copolymer

Films. *Sci. Rep.* **2014**, *4*, 1–8.

Graphic for manuscript